Systems/Circuits

Multielectrode Cortical Stimulation Selectively Induces Unidirectional Wave Propagation of Excitatory Neuronal Activity in Biophysical Neural Model

Alma S. Halgren,[1,2] **Zarek Siegel,**[1,3] **Ryan Golden,**[1,3] **and Maxim Bazhenov**[1,3]

[1]Department of Medicine, University of California - San Diego, La Jolla, California 92093-7374, [2]Department of Integrative Biology, University of California - Berkeley, Berkeley, California 94720, and [3]Neurosciences Graduate Program, University of California - San Diego, La Jolla, California 92093-7374

Cortical stimulation is emerging as an experimental tool in basic research and a promising therapy for a range of neuropsychiatric conditions. As multielectrode arrays enter clinical practice, the possibility of using spatiotemporal patterns of electrical stimulation to induce desired physiological patterns has become theoretically possible, but in practice can only be implemented by trial-and-error because of a lack of predictive models. Experimental evidence increasingly establishes traveling waves as fundamental to cortical information-processing, but we lack an understanding of how to control wave properties despite rapidly improving technologies. This study uses a hybrid biophysical-anatomical and neural-computational model to predict and understand how a simple pattern of cortical surface stimulation could induce directional traveling waves via asymmetric activation of inhibitory interneurons. We found that pyramidal cells and basket cells are highly activated by the anodal electrode and minimally activated by the cathodal electrodes, while Martinotti cells are moderately activated by both electrodes but exhibit a slight preference for cathodal stimulation. Network model simulations found that this asymmetrical activation results in a traveling wave in superficial excitatory cells that propagates unidirectionally away from the electrode array. Our study reveals how asymmetric electrical stimulation can easily facilitate traveling waves by relying on two distinct types of inhibitory interneuron activity to shape and sustain the spatiotemporal dynamics of endogenous local circuit mechanisms.

Key words: **biophysical model; cortical simulation; multielectrode arrays; network model; stimulation**

Significance Statement

Electrical brain stimulation is becoming increasingly useful to probe the workings of brain and to treat a variety of neuropsychiatric disorders. However, stimulation is currently performed in a trial-and-error fashion as there are no methods to predict how different electrode arrangements and stimulation paradigms will affect brain functioning. In this study, we demonstrate a hybrid modeling approach, which makes experimentally testable predictions that bridge the gap between the microscale effects of multielectrode stimulation and the resultant circuit dynamics at the mesoscale. Our results show how custom stimulation paradigms can induce predictable, persistent changes in brain activity, which has the potential to restore normal brain function and become a powerful therapy for neurological and psychiatric conditions.

Introduction

Brain stimulation is widely used in both experimental and clinical settings. In basic research, it is used to probe neural function by disrupting or hyperactivating local brain processing (E. Halgren et al., 1978; Salzman et al., 1990; Tehovnik et al., 2002). In clinical settings, direct manipulation of activity via stimulation has also been shown to be effective in the treatment of several neurological and psychiatric disorders. Deep brain stimulation (DBS) has been successful in the treatment of movement disorders, such as Parkinson's disease (Blumenfeld and Bronte-Stewart, 2015; Baizabal-Carvallo and Alonso-Juarez, 2016; Papageorgiou et al., 2017), depression (Mayberg et al., 2005; Schlaepfer et al., 2008), and obsessive-compulsive disorder (Abelson et al., 2005; B. D. Greenberg et al., 2006). Superficial cortical stimulation is an effective therapy for epilepsy (Nagaraj et al., 2015) and stroke patients (Hummel and Cohen, 2006). Increasingly, electrical

Received Sep. 1, 2021; revised Dec. 27, 2022; accepted Jan. 13, 2023.

Author contributions: A.S.H., Z.S., R.G., and M.B. designed research; A.S.H. and Z.S. performed research; A.S.H., Z.S., and R.G. analyzed data; A.S.H. wrote the first draft of the paper; A.S.H., R.G., and M.B. edited the paper; A.S.H., Z.S., and M.B. wrote the paper.

This work was supported by National Institutes of Health, National Institute of Neurological Disorders and Stroke Grant 1R01NS109553 and National Institutes of Health, National Institute of Mental Health Grant 1RF1MH117155.

The authors declare no competing financial interests.

Correspondence should be addressed to Maxim Bazhenov at mbazhenov@ucsd.edu.

https://doi.org/10.1523/JNEUROSCI.1784-21.2023

stimulation has also shown promise in both the restoration and enhancement of critical cognitive functions, such as memory. DBS has been shown experimentally to enhance memory encoding when applied during learning (Suthana et al., 2012), and closed-loop stimulation protocols have proven to be effective during periods of poor memory encoding as well as during memory recall (Ezzyat et al., 2018; Kahana et al., 2018; Kucewicz et al., 2018a,b).

While brain stimulation is sometimes conceptualized as disrupting pathological activity to restore normal activity, increasingly the explicit goal is to directly generate normal activity. Experimental evidence supports traveling waves as critical to normal brain activity. These propagating waves are fundamental to brain information-processing as they coordinate neural behavior across all spatial scales, from within-layer to whole-brain interactions, as well as across temporal scales, from tens to hundreds of milliseconds. By mediating communication across multiple brain areas, propagating activity putatively performs a variety of cognitive functions, such as the processing of visual stimuli or long-term memory consolidation (Muller et al., 2018). For example, sleep spindles traveling across the cortical surface at multiple scales have been hypothesized to synchronize convergent co-firing of neurons, resulting in spike timing-dependent plasticity and consequent memory consolidation (Dickey et al., 2021). Similarly, the alpha rhythm which modulates visual processing appears to be a traveling wave from association to primary areas (M. Halgren et al., 2019). Accordingly, the ability to predict and control traveling waves has far-reaching implications for improving and controlling cognitive function.

Currently, there is no method for reliably generating directional traveling waves with electrical stimulation. Past efforts to develop new paradigms of stimulation which reinstate particular brain activity states have largely depended on trial and error. Recently, we described a method for modeling the effects of cortical stimulation that enables one to predict the consequences of stimulation *in silico*, and thereby develop stimulation protocols that achieve desired results *in vivo* (Komarov et al., 2019). This earlier study was limited to the effects of stimulation of a single electrode and thus did not evoke directional propagation. In this new study, we describe an initial attempt to model a multielectrode stimulation paradigm that produces unidirectional traveling waves in the cortex. With multielectrode arrays increasingly entering clinical practice (Ha et al., 2017), our model harnesses the additional complexity and control during stimulation that multielectrode protocols allow for.

This modeling approach includes two phases. In the first phase, a biophysical model is used to predict spiking probability in response to a spatially-varied electric field potential in reconstructed rat somatosensory cortical neurons obtained from www.neuromorpho.org (Ascoli et al., 2007). We found that the hyperpolarization or depolarization of individual neurons varied according to cell type and cortical depth, and also varied with respect to the polarity of the applied electric field. The diversity in excitation responses underlies the propagating wave activity that we observed in the second phase of the model. In this second phase, we constructed a Hodgkin–Huxley model of a rat somatosensory cortical network composed of multiple interconnected cortical columns, each containing a circuit of inhibitory and excitatory cells connected within and across cortical layers. Approximating stimulation effects using the activation probabilities calculated in Phase 1, we found that fast inhibitory activity, coupled with excitatory cells' preference for anodal stimulation, resulted in a unidirectional, propagating wave of activity. Importantly, we found that the temporal component of the wave (the timing of cell firing within the excitatory-inhibitory feedback loop) resulted from an interaction between pyramidal and basket inhibitory cells, suggesting that a brief pulse of suprathreshold amplitude is sufficient to facilitate oscillatory activity thought to be endogenous to cortical columnar circuits. The spatial component (asymmetry) of the wave, however, was shown to depend on the unique activation profile of Martinotti inhibitory cells under this stimulation paradigm relative to the pyramidal and basket cells. These results suggest a simple multielectrode pattern for evoking traveling waves and provide testable predictions for experimental confirmation and parameter optimization.

Table 1. Summary of datasets with reconstructed cells[a]

Cell type	No. of reconstructions	Reference	Strain (age)
Pyramidal cells (Layer II/III)	21	Tehovnik et al., 2006	Wistar (P20-P25)
Pyramidal cells (Layer IV)	11	Traub et al., 1994	Wistar (P19-P21)
Pyramidal cells (Layer Va)	14	Wang et al., 2002	Wistar (P20-P21)
Basket cells (Layer II/III)	96	Wester and Contreras, 2012	Wistar (P13-P15)
Basket cells (Layer IV)	82	Wester and Contreras, 2012	Wistar (P13-P15)
Basket cells (Layer V)	57	Wester and Contreras, 2012	Wistar (P13-P15)
Martinotti cells (Layer II/III)	13	Douglas and Martin, 1991	Wistar (P13-P16)
Martinotti cells (Layer V)	7	Douglas and Martin, 1991	Wistar (P13-P16)
Horizontal interneurons (Layer I)	59	Wang et al., 2004	Wistar (P13-P16)
Descending interneurons (Layer I)	29	Wang et al., 2004	Wistar (P13-P16)
Small interneurons (Layer I)	27	Wang et al., 2004	Wistar (P13-P16)

[a]Cell types (from www.neuromorpho.org) that were used in the biophysical component of the model.

Materials and Methods

Cell reconstruction selection. All neuronal cell reconstructions were chosen from publicly available datasets on www.neuromorpho.org (Wang et al., 2002, 2004; Staiger et al., 2004; Schubert et al., 2006; Ascoli et al., 2007; Muralidhar et al., 2013). The types of cells and their respective datasets are listed in Table 1. We used multiple cell reconstructions for each cell type to account for anatomical diversity. We used experimental measurements to approximate the cutoff depths for each layer (see Fig. 1*a*) (Markram et al., 2004; Wang et al., 2004).

Calculating the electric field potential generated by the electrode array. The electrode array modeled in this study was composed of three square electrodes (each 150 μm × 150 μm) placed linearly on the surface of the cortex. Two electrodes had negative current (−75 μA each) and one electrode had positive current (150 μA) (see Fig. 1*a*), and stimulation was applied for 200 μs. This was done to adhere to the constraints of clinical applications of electrical stimulation which require a net neutral current to be delivered to the tissue. These values are in accordance with common experimental parameters (Ha et al., 2017). Assuming that the current sources are homogeneous square electrodes, we calculated the electric field potential of each electrode as follows:

$$\Phi(X,Y,Z) = \frac{\rho_e I}{4\pi A^2} \iint_{-A/2}^{A/2} \frac{\mathrm{d}x\mathrm{d}y}{\sqrt{(X-x)^2+(Y-y)^2+Z^2}} \quad (1)$$

Here I is net current, ρ_e is extracellular resistivity, and A is the length of the square electrode edge (see Fig. 1*a*). In this study, $A = 150\,\mu$m and net current I is either −75 or 150 μA. The derivation of this formula can be found in our previous work (Komarov et al., 2019). We summed all three electric field potentials at each point in space to determine the overall electric field potential.

Estimating the activating function. This paper used a similar approach to that of Komarov et al. (2019) to estimate the firing probability for each neuronal reconstruction. The basis of this approach is the activating function, a formula derived from cable theory that describes the effective transmembrane current that arises because of extracellular

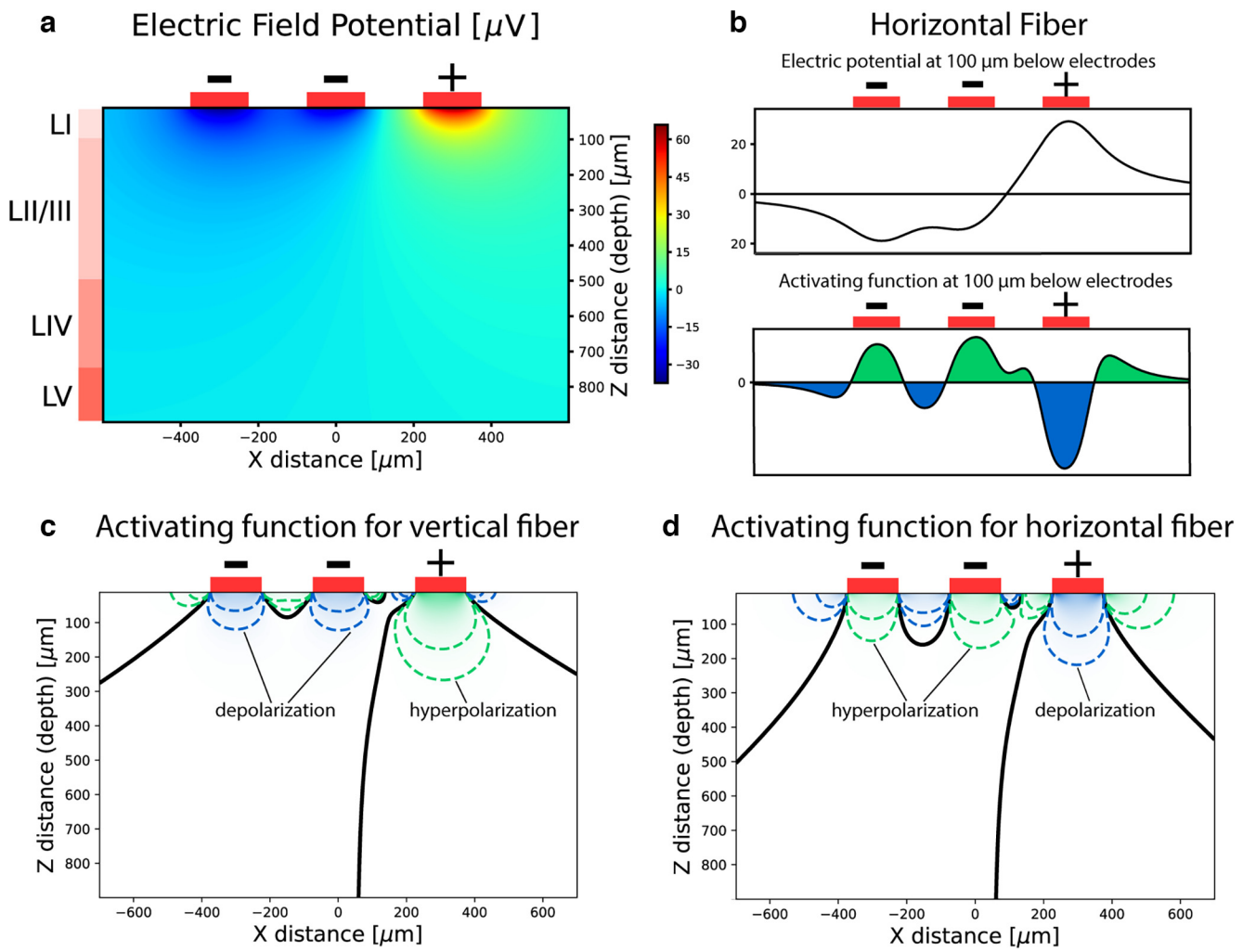

Figure 1. Electric potential and activating function in the plane $Y = 0$. ***a***, Schematic of the electrode configuration and electric potential in the plane $Y = 0$. Each electrode is square-shaped and measures 150 μm × 150 μm, and the spacing between each electrode is also 150 μm. The two leftmost electrodes are negative (cathodal) and deliver negative 75 μA of current each, while the rightmost electrode is positive (anodal) and delivers 150 μA of current, and the stimulation period is 200 μs. Layer depths are approximated from experimental measurements of rat cortex (Markram et al., 2004; Wang et al., 2004; Defelipe et al., 2012) as follows: layer I is 0-100 μm, layer II/III is 100-500 μm, layer IV is 500-750 μm, and layer V is 750-900 μm. ***b***, Axial potential along a horizontal axonal fiber located 100 μm below the cortical surface. The activating function is the second spatial derivative of the electric potential. ***c***, ***d***, As a result of ***b***, horizontal fibers are activated by the anode and hyperpolarized by the cathodes (***d***). The opposite is true for vertical fibers (***c***). The vast majority of direct stimulation occurs in layers I and II/III because of the decay of electric potential with depth.

electrical stimulation. This was used to calculate the transmembrane voltage in each axonal segment of every cell reconstruction. We then applied a threshold of activation to determine whether an axonal response was triggered. This threshold was drawn from *in vivo* experiments which define the threshold injected current I required to induce a threshold effective current f at the axonal initial segment located at a distance d from the electrode (Douglas and Martin, 1991; R. J. Greenberg et al., 1999). In previous work (Komarov et al., 2019), we simulated one such experiment by computing the activation current f at the axon initial segment of a layer II/III pyramidal cell while varying the stimulation current I and distance d. This simulation used a 200 μs-duration stimulating pulse, which is typical of similar *in vivo* experiments (Douglas and Martin, 1991; R. J. Greenberg et al., 1999). The value $f = f_{th} = 3\,\text{pA}/\mu\text{m}^2$ fully replicated the experimentally-observed current-distance relationship across varying stimulation currents and distances. Thus, this threshold value f_{th} was used to determine whether each axonal segment was activated by induced transmembrane current.

Since we compute the activating function in each small compartment composing an entire axonal arborization, jitter in the edges of the anatomical reconstruction could introduce numeric noise in our calculation. To minimize this issue, we estimate the direction of each axonal component (the mini segment forming a compartment in the reconstruction) using the position in space of neighboring compartments up to 10 μm away. The estimated direction is then crucial to computing the activating function, which, by definition, is calculated along the axonal element direction.

An important note is that this protocol neglects the effects of axonal branching at adjacent segments. Instead, it acts as though the axon continued, unbranched, in a direction given by the sum of the two orientation vectors of the bifurcated segments. However, given that we base our activation probabilities (see Computing the average activation probability per cell type below) on the total length of activated segments within a reconstruction, and then average across all reconstructions of that cell type, we believe that this impact is negligible.

Computing the average activation probability per cell type. To determine whether a given neuronal reconstruction would be activated by applied current, we used the activating function to calculate how many axonal segments had above-threshold transmembrane current values that could initiate an axonal action potential (assumed at nodes of Ranvier); these above-threshold axonal segments are collectively called the trigger area. The activating function threshold was set to $f_{th} = 3\,\text{pA}/\mu\text{m}^2$ for myelinated axons and to $f_{th} = 60\,\text{pA}/\mu\text{m}^2$ for unmyelinated

axons, since unmyelinated segments are significantly less excitable as they have fewer sodium channels (Cogan et al., 2016). In this model, we assumed pyramidal and basket cells are myelinated and Martinotti and layer I interneurons are unmyelinated based on experimental data (Thomson et al., 2002; Wang et al., 2004; Tomassy et al., 2014). For each cell reconstruction at a given point in space (i.e., a given coordinate in the *x*-*z* plane; see Fig. 1*a*), we found the probability of firing as outlined in prior work (Komarov et al., 2019). Given that variation in cell position and orientation within each cortical layer are present in nature, we additionally average across neuronal rotations and vertical shifts. Thus, we computed the average activation probability for each cell type/cortical layer pairing as follows: for each cell reconstruction, we first positioned the soma at a point along the *x* axis within its cortical layer. We then performed four rotations (0°, 90°, 180°, and 270°) about the vertical axis of the cell reconstruction in three-dimensional (3D) space, and at every rotation we calculated the likelihood of activation by computing the activating function across the axonal arbor, as outlined above. We then averaged across these four probabilities and set the result as the activation probability for said point. After this, we incrementally shifted the soma of the reconstruction vertically within its cortical layer and found the mean activation probability at each point. We averaged across all vertical shifts within the cortical layer to obtain an approximate spiking probability for this cell reconstruction at this point along the *x* axis. Along the *x* axis, we computed the activation probability of all cell reconstructions and then averaged across all cell reconstructions within a given cell type and cortical layer (see Fig. 3).

Computational model of the cortical circuit. The network model is composed of 11 interconnected cortical columns, where each column contains layer I interneurons and pyramidal, basket, and Martinotti cells from layers II-V (same as the biophysical analysis). The number of cells within each column is outlined in Table 2. This balance of excitatory to inhibitory cell types approximates the true cell composition of the rat somatosensory cortex, where pyramidal cells are the primary excitatory cells and basket and Martinotti cells comprise the majority of inhibition within and across layers (Markram et al., 2004; Wang et al., 2004). Cells were constructed to only spike if receiving synaptic input or electrical stimulation. Each cell behaves according to Hodgkin–Huxley dynamics, with a handful of parameters differentiating excitatory and inhibitory cells. Basket cells were modeled as fast-spiking cells, while all other cell types were modeled as regular-spiking cells with spike rate adaptation. Inhibitory cells fired more quickly than excitatory cells in response to activation because all interneurons were modeled as having a lower leak current than excitatory cells (Santos et al., 2012). Some additional parameters were as follows: a fast Na^+-K^+ spike generating mechanism (all cells), a high-threshold activated Ca^{2+} current (for pyramidal cells), and a slow calcium-dependent potassium (AHP) current (for regular-spiking cells).

The network architecture and function mirror that of Komarov et al. (2019) with the following exceptions: first, our network contains multiple columns while that in Komarov et al. (2019) only contains one; second, the initial activation probabilities in our network are derived from the first phase of our model (see Fig. 3) instead of from the probabilities calculated in prior work (Komarov et al., 2019); and third, our model contains slightly different cells (e.g., layer I cells) than those included previously (Komarov et al., 2019). The Hodgkin–Huxley equations that govern the dynamics of our model can be found in our prior work (Komarov et al., 2019).

Initially, the network runs without stimulating input for 200 ms to simulate preexisting activity. Then the network is stimulated and runs for an additional 500 ms. To simulate electrical stimulation, we used the binary term I_i^{ext} to inject above-threshold current into a subset of randomly chosen neurons within each cell type/cortical layer pairing such that the fraction of neurons induced to spike corresponds to the activation probabilities calculated in the biophysical phase of the model (see Fig. 3). For neurons in columns 1-3 and 9-11, the activation probabilities were set to zero. This was because the electric field generated by the electrode design was effectively null at locations this far from the stimulating electrodes. The term $\eta\xi_i(t)$ models spontaneous background activity as a white noise process (ξ) with SD η. All model parameters are listed in Komarov et al. (2019, their Table S2) (unless specified in the description of simulations), and the network structure and connectivity are described in Table 2 and Table 3, respectively. Cells were synaptically coupled by excitatory (AMPA) and inhibitory ($GABA_A$) connections. The strength and probability of connections between layers and cell types were set according to a canonical cortical circuit (Thomson et al., 2002).

Average network activity. To quantify network behavior across 50 simulations per current strength, we averaged the percentage of spiking across all cell types at each cortical column (see Fig. 5*c*).

Table 2. Structure of the network[a]

Cortical cell type	Layer	Cells/column	Total cells
IN	I	12	132
PY	II/III	100	1100
BC	II/III	100	1100
MC	II/III	24	264
PY	IV	12	132
BC	IV	12	132
MC	IV	12	132
PY	V	12	132
BC	V	12	132
MC	V	12	132
Total		308	3388

[a]The layer, cells per column, and total cells per cell type used in the network model.

Table 3. Connectivity within the network[a]

Presynaptic		Postsynaptic					
Type	Layer	Type	Layer	Cross-column	Type	Strength	Probability
PY	II/III	PY	II/III	True	AMPA	0.4	0.1
PY	IV	PY	IV	True	AMPA	0.4	0.1
PY	V	PY	V	True	AMPA	0.4	0.1
PY	II/III	PY	II/III	False	AMPA	0.75	0.1
PY	II/III	BC	II/III	False	AMPA	0.75	0.1
PY	II/III	MC	II/III	False	AMPA	0.75	0.1
PY	II/III	PY	IV	False	AMPA	0.25	0.05
PY	IV	PY	II/III	False	AMPA	1.5	0.05
PY	IV	PY	IV	False	AMPA	0.75	0.1
PY	IV	BC	IV	False	AMPA	0.75	0.1
PY	IV	MC	IV	False	AMPA	0.75	0.1
PY	IV	BC	II/III	False	AMPA	1.5	0.05
PY	IV	MC	II/III	False	AMPA	1.5	0.05
PY	V	PY	V	False	AMPA	0.75	0.1
PY	V	PY	II/III	False	AMPA	0.5	0.05
PY	V	BC	V	False	AMPA	0.75	0.1
PY	V	MC	V	False	AMPA	0.75	0.1
MC	II/III	PY	II/III	False	GABA	0.75	0.05
MC	II/III	PY	IV	False	GABA	0.75	0.05
MC	II/III	PY	V	False	GABA	0.75	0.05
MC	IV	PY	II/III	False	GABA	0.75	0.05
MC	IV	PY	IV	False	GABA	0.75	0.05
MC	IV	PY	V	False	GABA	0.75	0.05
MC	V	PY	II/III	False	GABA	0.75	0.05
MC	V	PY	IV	False	GABA	0.75	0.05
MC	V	PY	V	False	GABA	0.75	0.05
BC	II/III	PY	II/III	False	GABA	1.5	0.25
BC	IV	PY	IV	False	GABA	1.5	0.25
BC	V	PY	V	False	GABA	1.5	0.25
MC	V	PY	IV	False	GABA	1	0.2
MC	V	PY	V	False	GABA	1.5	0.25
IN	I	PY	II/III	False	GABA	0.3	0.3
IN	I	PY	IV	False	GABA	0.3	0.3
IN	I	PY	V	False	GABA	0.3	0.3
PY	II/III	IN	I	False	AMPA	0.3	0.3

[a]Type, strength, and probability of connections between all cell types and layers. These values were estimated from experimental data of anatomic connectivity across slices of the rat cortex (Thomson et al., 2002).

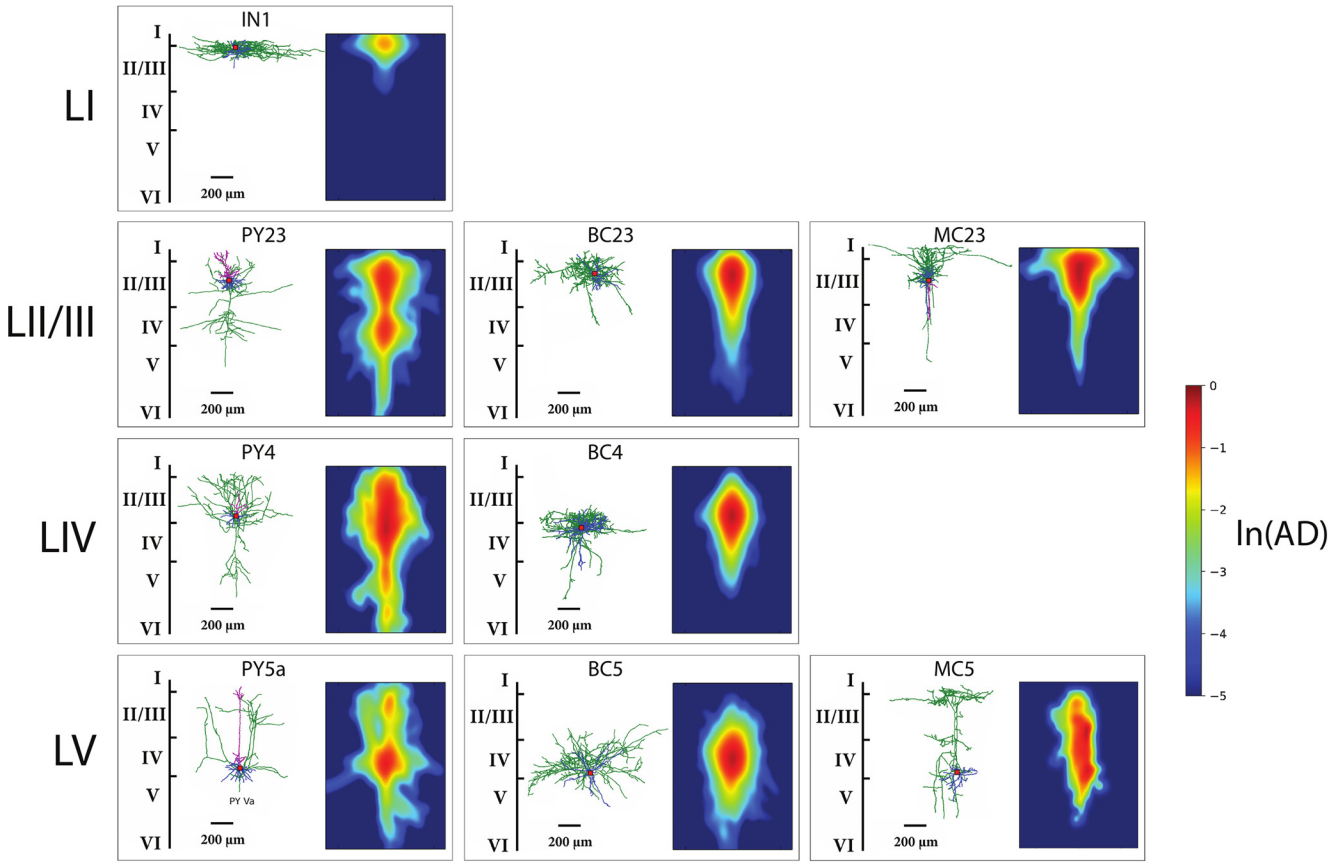

Figure 2. Representative reconstructions and averaged axonal density for neuronal cell types modeled. For each neuronal cell type used in the cortical microcircuit model, we plot both a single representative anatomical reconstruction as well as an averaged axonal density heatmap for all the reconstructions of that type. Cells are arranged by layer and type; the first row represents layer I inhibitory neurons. The representative layer I interneuron is a horizontal cell, but we average across small, descending, and horizontal layer I interneurons in both the axonal heatmap as well as in our analyses. The following rows represent pyramidal, basket, and Martinotti cells across layers II/III, IV, and V (layer Va for pyramidal cells). We did not have neuronal reconstructions for layer IV Martinotti cells and averaged spiking probability results from layers II/III and layer V Martinotti cells for subsequent analyses. In the axonal density (AD) plots, color represents the averaged density computed using all available reconstructions for the given cell type. The color scale is logarithmic for visual clarity. AD gives a sense of the general orientation and density of axon branches for each cell type, which is key to understanding subsequently computed activation probabilities.

Results

Building upon existing *in silico* models that simulated the effects of cortical surface stimulation from a single electrode (Komarov et al., 2019), in this study we sought to explore the spatial dynamics of stimulation by modeling an asymmetrical three-electrode configuration applied to the rat somatosensory cortex (Fig. 1*a*). This configuration was initially chosen to break the symmetry between the anodal and cathodal currents and pursued further because of the wave propagation observed in the network model as a result of the electrode choice. The paper is organized as follows. We first calculated the electric field potential created by the system of three electrodes: two cathodes (at -75 μA each) and a single anode (at 150 μA). Next, we estimated the activation probability for each cell type/cortical layer pairing by computing the activating function in biophysical reconstructions of axonal arbors. We then constructed a cortical microcircuit model with Hodgkin–Huxley dynamics to model the network effects of stimulation based on the previously-calculated spiking probabilities.

Cell activation results from a combination of morphology (cell type) and depth within the column

The applied electric field potential generated by the system of three electrodes (assuming homogeneous tissue) is shown in Figure 1*a*. To estimate the probability of specific cell types being activated by stimulation, we simulated the various cell types based on 3D morphological reconstructions of neurons derived from electron microscopy available from www.neuromorpho.org (Ascoli et al., 2007). The excitatory cells we considered were pyramidal cells across layers II-V, while the inhibitory neurons included basket cells and Martinotti cells across layers II-V in addition to layer I interneurons (Table 1). Example reconstructions as well as average axon density plots per cell type/cortical layer (Fig. 2) demonstrate the significant differences in axonal arborization and density among the different cell types, as well as between cells of the same type based in different layers.

The hyperpolarization or depolarization of a neuronal fiber within a constant electric field can be modeled with one-dimensional cable theory in conjunction with the activating function. The activating function (for details, see Materials and Methods) (Komarov et al., 2019) computes the net transmembrane current generated by external stimulation (while ignoring preexisting synaptic currents). According to one-dimensional cable theory, the activating function is the second-order spatial derivative of the electric potential along the neuronal fiber. The case of a perfectly horizontal fiber is shown in Figure 1*b*. Through this, we can draw relationships between the orientation and excitation of a fiber in response to a given stimulation polarity. Indeed, horizontal fibers were depolarized by anodal stimulation and hyperpolarized

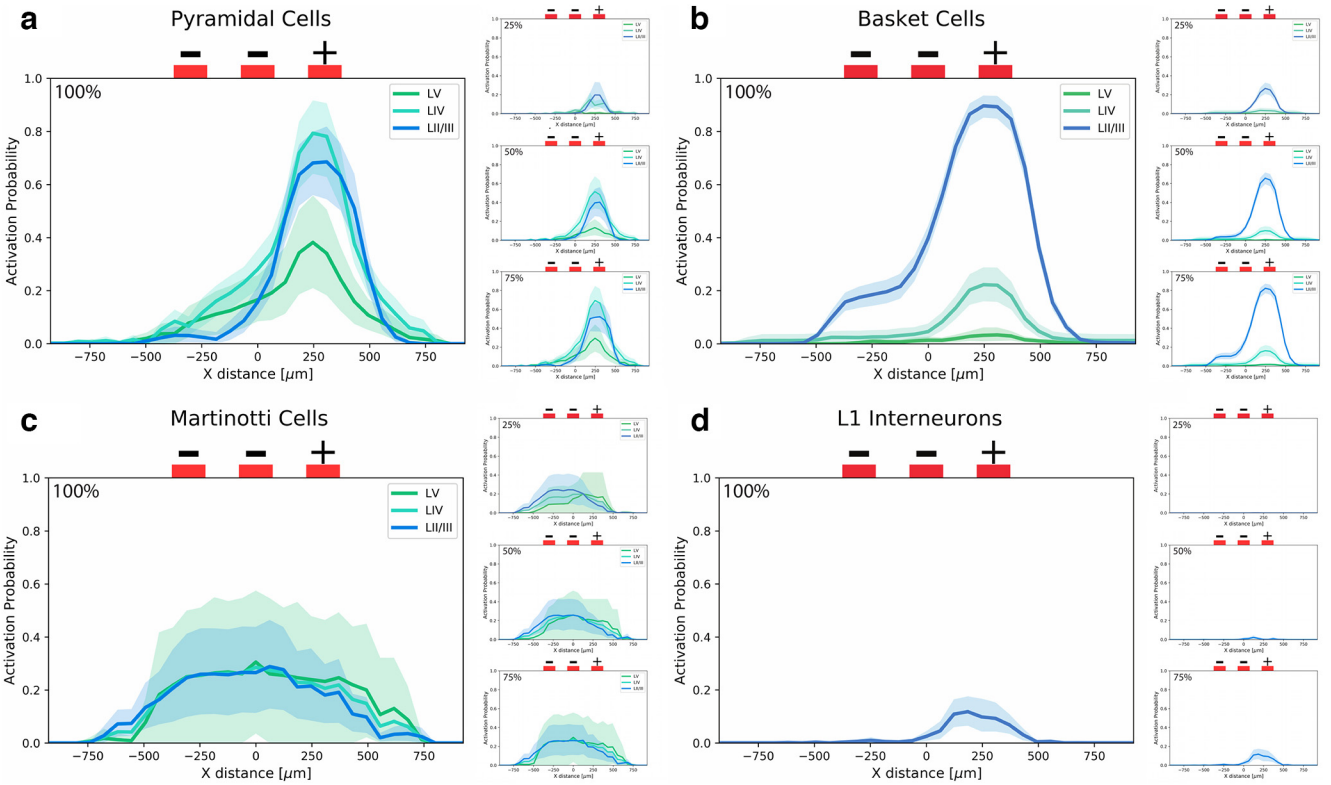

Figure 3. Probability of spiking as a function of horizontal distance from the center of the electrode array for each cell type and cortical layer. Average (solid line) cell spiking probability and 95% confidence intervals (shaded region) for each reconstruction were calculated for soma locations across the entire *X-Z* plane of the corresponding cortical layer by averaging spiking probability across rotations and vertical shifts of all cell reconstructions. Activation probabilities were calculated across four stimulating current strengths, with the maximum anodal stimulation current set to 150 μA and the maximum cathodal stimulation current set to -75 μA per electrode over a 200 μs stimulation period. Right, Insets, Activation profiles for 25%, 50%, and 75% stimulation strength. Pyramidal cells (excitatory, ***a***) and basket cells (inhibitory, ***b***) are highly activated by anodal stimulation and are minimally activated by cathodal stimulation because of their myelination and horizontally oriented axonal arbors. Martinotti cells (inhibitory, ***c***) are activated by all electrodes with a slight preference for the cathodes but lack myelination and thus show less activation overall. Layer I interneurons (***d***) are also unmyelinated and are minimally excited by stimulation.

by cathodal stimulation; in contrast, vertical fibers were hyperpolarized by anodal stimulation and depolarized by cathodal stimulation (Fig. 1*d* and Fig. 1*c*, respectively). While each neuron has unique axonal fibers that span 3D space, these maps of activation and suppression zones for orthogonal axonal orientations give us insight into how each cell type will behave across the stimulated space given its average axon density and orientation (Fig. 2).

We next calculated spiking probability in response to the applied electric field potential for each cell type/cortical layer pairing by averaging across the activating function results of their respective cell reconstructions; each cell reconstruction was shuffled by rotating and shifting along the vertical axis, and multiple reconstructions were considered for each cell type (for details, see Materials and Methods) (Komarov et al., 2019). This calculation compares the overall excitability of each reconstruction to an experimentally derived threshold (f_{th} = 3 pA/μm^2) to determine the probability of spiking. This threshold was set 20 times higher for unmyelinated cell types (Martinotti cells and layer I interneurons) compared to myelinated cell types (pyramidal and basket cells) since unmyelinated fibers are relatively unexcitable and lack nodes of Ranvier (Markram et al., 2004; Wang et al., 2004; Defelipe et al., 2012). The results of these calculations are shown in Figure 3.

To explore the parameter space of the model, we calculated activation probabilities at 25%, 50%, and 75% of the maximum stimulation current (150 μA for the anode and -75 μA for each cathode), which are displayed in Figure 3. The activation probabilities scale upward with increasing applied current for all cell types except Martinotti. At the weakest applied current, at which the absolute values of current amplitudes are <50 μA, layer II/III Martinotti cells exhibit a slight preference for cathodal stimulation, layer V Martinotti cells exhibit a slight preference for anodal stimulation, and layer IV cells show no strong preference. However, at all currents above the weakest, Martinotti cells across all layers display a slight preference for cathodal stimulation, and the activation probabilities appear to have reached a plateau; that is, increasing the applied current increases activation probabilities for all cell types except Martinotti. The average axonal density heatmaps in Figure 2 as well as the presence or absence of myelination explain the variation of activation responses across cell types and cortical layers.

Across all layers, pyramidal cells were strongly activated by the anode and minimally activated by the cathodes, with layer IV showing the greatest, layer V the least, and layer II/III an intermediate probability of activation (Fig. 3*a*). As shown in Figure 2, all pyramidal cells vertically span the cortical layers regardless of soma position. However, layer II/III and layer IV pyramidal cells exhibit significant horizontal axonal density close to the cortical surface and thus responded more strongly to stimulation overall (and to cathodal stimulation in particular), whereas the bulk of layer Va pyramidal axons lie in deeper layers and lack the superficial axonal density to be adequately stimulated above threshold. Pyramidal cells display a strong overall response to stimulation due to their myelinated axons.

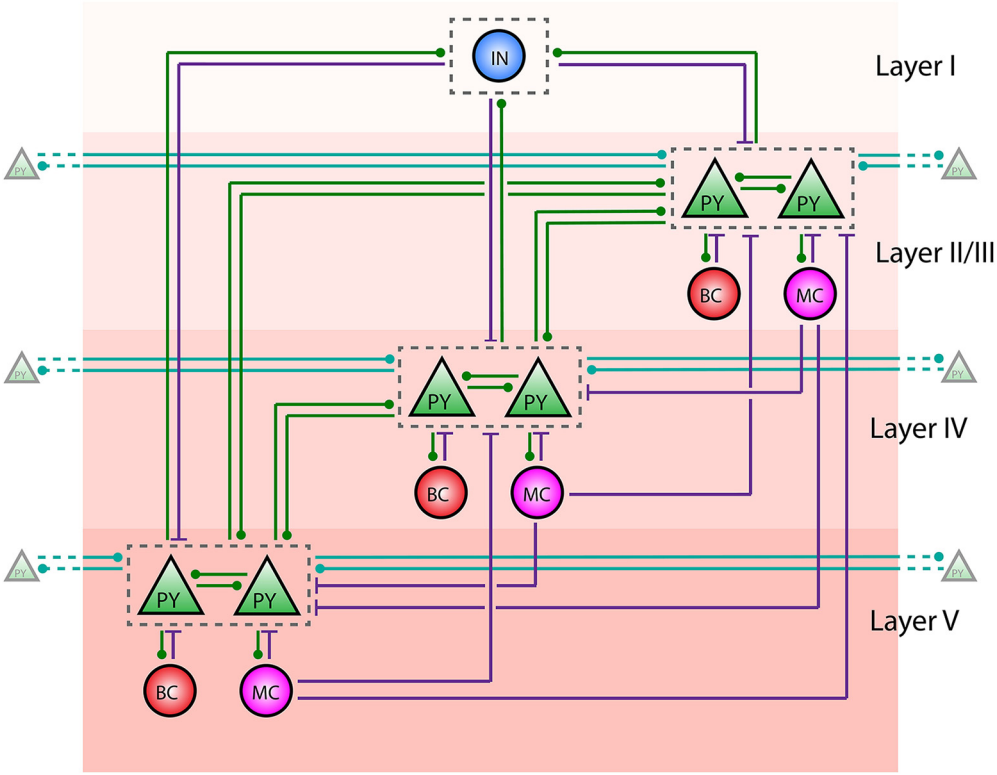

Figure 4. Microcircuit diagram of a single cortical column in modeled network. This depiction of a single cortical column details the cell types across cortical layers and the synaptic connections between them in our microcircuit network model. Circular labels (IN, LI interneurons; BC, basket cells; MC, Martinotti cells) represent inhibitory neurons. Triangular labels (PY, pyramidal cells) represent excitatory neurons. Green connections represent excitatory synapses, with the circular end indicating the postsynaptic cell and the unlabeled end indicating the presynaptic cell. Purple connections represent inhibitory synapses, with the perpendicular line indicating the postsynaptic end. Teal-colored connections are also excitatory but represent connections from pyramidal cells to others in adjacent columns (cross-columnar synapses). The gray box that surrounds the pyramidal cells within each layer includes all synaptic connections to all pyramidal cells, not just the ones closest to the synapse in the figure. The only cross-column synapses present are within-layer pyramidal-pyramidal excitatory connections to adjacent columns. Layer I includes only inhibitory interneurons, which inhibit pyramidal cells in all three deeper layers and are reciprocally excited by the same cells. Each of the deeper layers contain pyramidal, basket, and Martinotti cells. Within a cortical column, pyramidal cells reciprocally excite other pyramidal cells in their same layer as well as across cortical layers. Basket cells act as local interneurons as they only inhibit and are excited by pyramidal cells within their own layer. In contrast, while Martinotti cells are only excited by pyramidal cells within their own layer, they universally inhibit pyramidal cells across all layers. In this model, inhibitory cells receive only excitatory synaptic inputs. The number of neurons in each column is listed in Table 2 and the probability and strength of each synaptic connection is listed in Table 3.

Basket cells also exhibited a strong preference for anodal stimulation and little activation underneath the cathodes (Fig. 3*b*). However, their responses were significantly more tiered according to cortical layer compared with pyramidal cells because basket cell arborization is localized within the same layer as the soma (Fig. 2). Their preference for anodal stimulation is due to their largely horizontal axonal arbor that stretches out within each layer. Basket cells were the only myelinated inhibitory cell type in our model and therefore demonstrated a significantly stronger spiking response overall relative to Martinotti or layer I interneurons.

Martinotti cells across all layers are moderately activated by both anodal and cathodal stimulation but showed a slight preference for the latter (Fig. 3*c*). This is because all Martinotti cells make universal connections with pyramidal cells via layer I (Fig. 2); therefore, the majority of their arborizations lie in vertical axonal fibers connecting the soma to layer I, with additional density spread out horizontally across layer I. However, they exhibited a dampened stimulation response overall because of their unmyelinated axons.

Last, since layer I axon fibers are unmyelinated and stay localized to layer I (resulting in mainly horizontal arborization), layer I interneurons displayed a slight preference for anodal stimulation but little activation overall (Fig. 3*d*).

Cortical microcircuit model shows directional propagation when stimulated with three electrode array

In the previous section, we estimated the activation probabilities of isolated neurons within an applied electric field. To understand how stimulation affects the dynamics between neurons and ultimately the overall dynamics of the cortex, we constructed and stimulated a network model of the cortex using simplified neuron models and previously-calculated activation probabilities. Each cortical column was modeled as a canonical microcircuit (Douglas et al., 1989; Thomson et al., 2002; da Costa and Martin, 2010; Defelipe et al., 2012) containing the same cell types and cortical layers as the biophysical analysis above. A schematic of the cell types across cortical layers and their synaptic connections is shown in Figure 4.

The only cross-column synapses present are pyramidal-pyramidal excitatory connections to adjacent columns. Layer I includes only inhibitory interneurons, which inhibit pyramidal cells in all three deeper layers and are reciprocally excited by the same cells. Each of the deeper layers contain pyramidal, basket, and Martinotti cells. Within a cortical column, pyramidal cells reciprocally excite other pyramidal cells in their same layer as well as across cortical layers. Basket cells act as local interneurons as they only inhibit and are excited by pyramidal cells within their own layer. In contrast, while Martinotti cells are

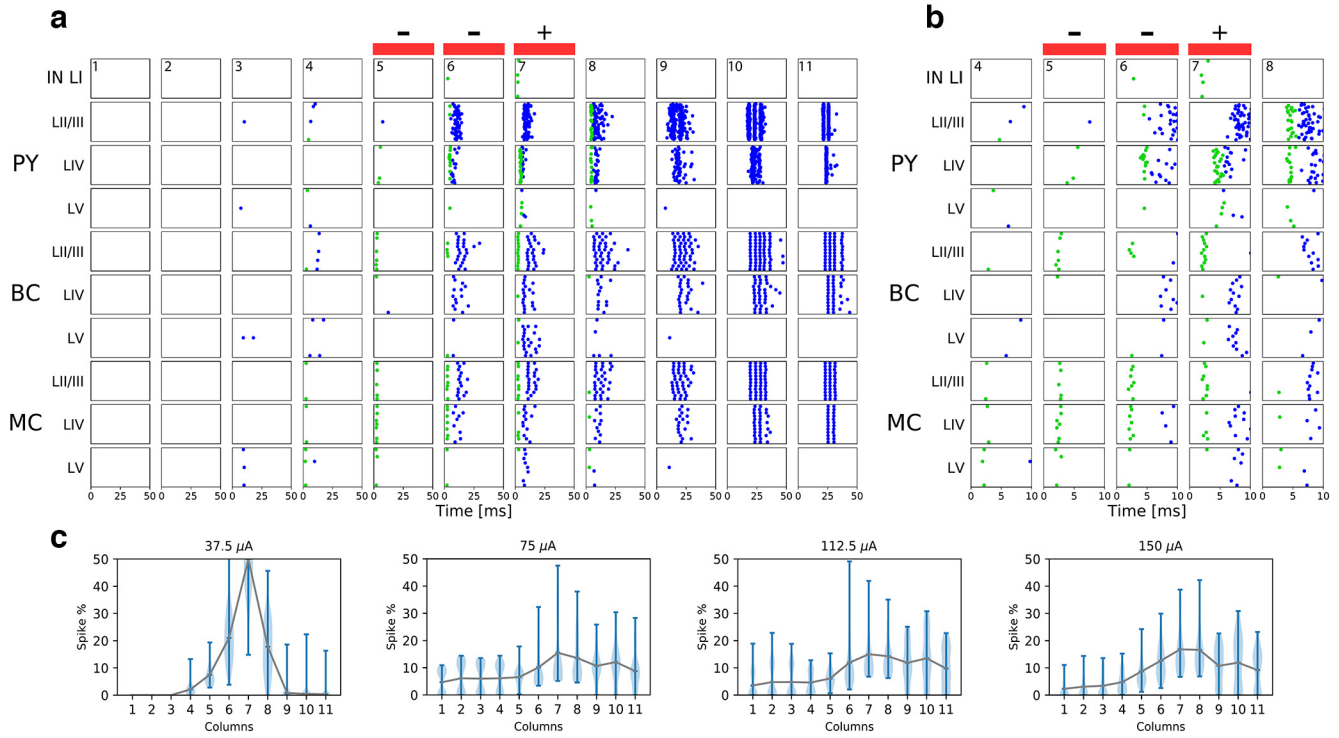

Figure 5. Directed propagation of pyramidal activity in raster plot of microcircuit simulation trial. A raster plot displaying network behavior during and after stimulation in one trial of the microcircuit simulation across all cortical columns at maximum applied current. Each cell within the microcircuit has its own coordinate on the *y* axis. Each dot is an action potential. Green dots indicate spikes that are directly triggered by electrical stimulation (occurs during first 5 ms). Blue dots indicate spikes triggered via synaptic input. ***a***, The first 50 ms of the simulation (the network is silent beyond this period). ***b***, Zoom in to the first 10 ms in the five central columns. ***c***, The percentage of spikes (all cell types) per cortical column, then averaged across 50 simulations at each applied current value (25%, 50%, 75%, and 100% applied current, with the anodal current listed, from left to right, respectively).

only excited by pyramidal cells within their own layer, they universally inhibit pyramidal cells across all layers. In this model, inhibitory cells receive only excitatory synaptic inputs. The number of neurons in each column is listed in Table 2 and the connectivity within the network is described in Table 3.

Following a brief stimulation period in which the activation probabilities from the biophysical calculations were applied to the model, the network was allowed to run without any external input for 500 ms, during which time it behaved according to synaptic interactions between neurons.

To test the robustness of network behavior, we conducted 50 simulations for four different values of stimulation current (25%, 50%, 75%, and 100% current, respectively) and calculated the percentage of total spikes in each cortical column averaged across these simulations (Fig. 5*c*). At the weakest applied current, spiking is highest underneath the anode and tapers off on either side as the stimulating current is not strong enough to induce propagating activity in either direction (Fig. 5*c*, leftmost plot). At ≥50% current, however, activity propagates unidirectionally as a traveling wave to the right. The following simulation example and subsequent explanations and analyses focus on network stimulation with the maximum current applied as it corresponds to strong asymmetric network behavior within physiological current bounds.

A raster plot and voltage and conductance traces of one microcircuit trial at maximum applied current are shown in Figures 5 and 6. The trial shown is one example of the general behavior of the microcircuit in the majority of trials at maximum applied current (Fig. 5*c*, rightmost plot) in which spiking activity, particularly from LII/III pyramidal cells, propagates to the rightward columns but not past the leftmost electrode. Given this unique spiking activity and the biological importance of LII/III pyramidal cells in mediating communication across cortical regions, we chose to focus our analyses on the network behavior of LII/III pyramidal cells.

Directionality of the stimulation-triggered wave can be explained by network inhibition

The activation probability curves in Figure 3 provide intuition into the network behavior during and immediately after the stimulation period (0-5 ms; Fig. 5*b*). Let us first examine the column underneath the anodal electrode (Fig. 5*b*, column 7). While both layer II/III and layer IV pyramidal cells were predicted to be highly activated underneath the anodal electrode (Fig. 3), only layer IV pyramidal cells were directly activated. Although all pyramidal cells were inhibited by moderate Martinotti activity, only layer II/III pyramidal cells were locally inhibited by strong synchronous layer II/III basket cell activity while other layers were not because basket cell response drops off with increasing cortical depth and because basket cells are only inhibit pyramidal cells within their own layer. Following stimulation, layer IV pyramidal cells excited layer II/III pyramidal cells and triggered a cluster of layer II/III activity. There was negligible layer V excitation during stimulation and none following because of their low excitation probabilities and relatively small neuronal population.

Network behavior underneath the cathodal electrodes contrasted sharply with anodal stimulation response and underpinned unidirectional excitatory propagation (Fig. 5*b*, columns 5 and 6). Although layers II/III and IV pyramidal cells were still moderately activated by cathodal stimulation (Fig. 3*a*), very few cells were pushed above threshold because of strong inhibition. Martinotti

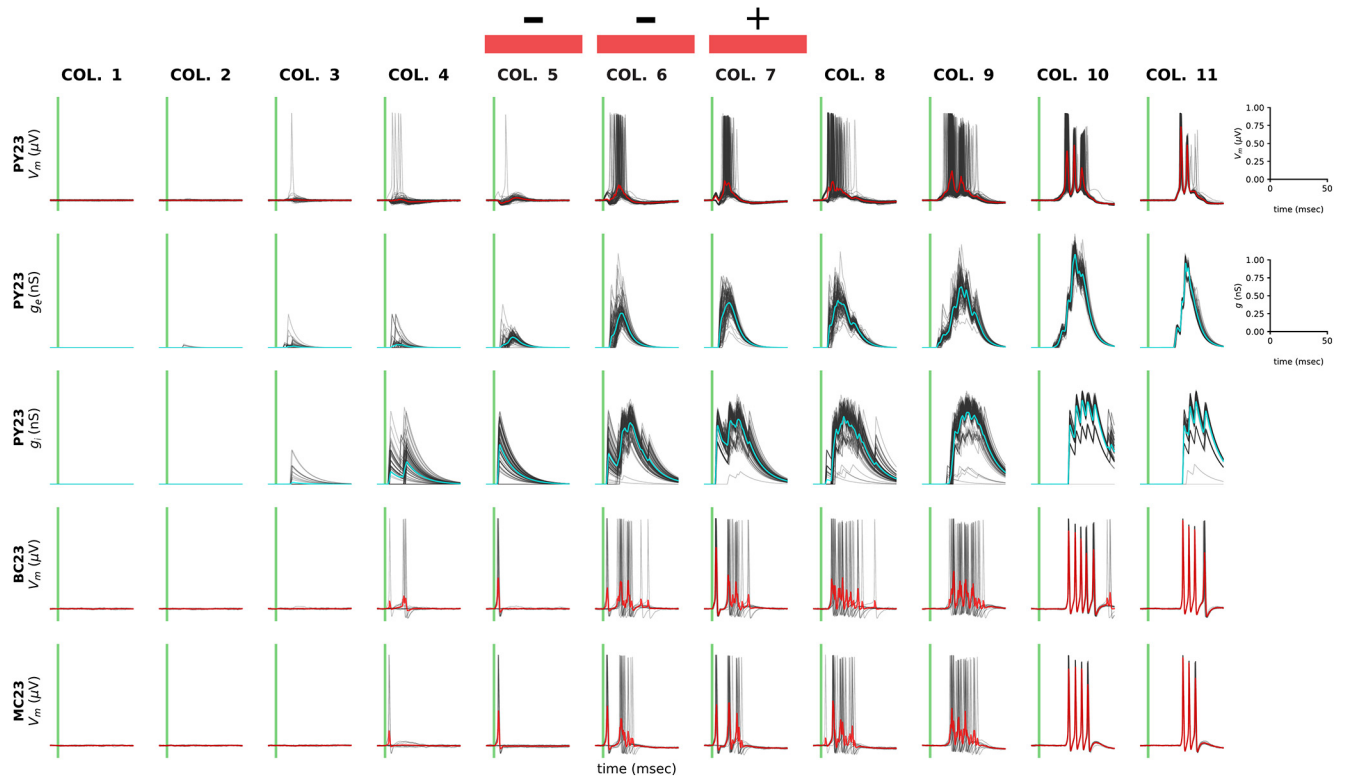

Figure 6. Voltage traces for layer II/III cells and pyramidal input conductances during simulation show how inhibition causes directionality of traveling wave. Each of the subplots in the grid contain data for the collection of layer II/III cells specified by type and column. The *x* axis for each subplot is time in milliseconds and is restricted to the interval from 5 ms before stimulation to 50 ms after. Region in light green represents stimulation period. Subplot columns, labeled at top, indicate the model columns. The first three rows represent data from pyramidal cells, with the first row representing the voltage trace, the second the total excitatory conductance (the sum of all incoming pyramidal connections), and the third the total inhibitory conductance (sum of inhibitory connections from layer I interneurons, basket cells, and Martinotti cells). The fourth and fifth rows represent the voltage traces of layer II/III basket and Martinotti cells, respectively. In each subplot, there are light gray traces representing each of the individual cells in the group, and their average (within the same column, layer, and subtype) in red. Sharp increases in the light gray trace indicate action potentials (spikes). Darker gray regions correspond to times when large numbers of cells spiked.

cells showed a preference for cathodal stimulation (according to Fig. 3) and thus fired early in the stimulation period, inhibiting pyramidal cells across all cortical depths (since Martinotti cells universally synapsed to all pyramidal cells in the network). This strong inhibitory force coupled with moderate superficial basket cell activity silenced almost all pyramidal activity across cortical layers.

In the column directly to the left of the electrode array (Fig. 5*b*, column 4), there was negligible activity across all cell types and cortical layers. Not only did the electric field potential drop off significantly at this distance, but pyramidal and basket cells were already minimally activated by the cathodal electrodes, and Martinotti cells were only moderately activated by the cathodal electrodes because of their lack of myelination. In the absence of stimulating electric field potential or activating input from neighboring cortical columns, the leftmost three columns exhibited no spiking activity at all (Fig. 5*a*, columns 1-3). Hence, the excitatory pyramidal activity present underneath the electrodes did not propagate leftward past the cathodal electrodes. This activity, however, did travel rightward past the electrode array, growing stronger and more synchronous as it propagated.

On the other side of the array, in the cortical column directly to the right of the anodal electrode (Fig. 5*b*, column 8), there was moderate direct activation of pyramidal cells and little direct activation of inhibitory cells. This follows from Figure 3, which depicts pyramidal cells continuing to be activated by the anodal electrode. While basket cells were also moderately activated by anodal stimulation, their joint inhibition with Martinotti cells was not enough to counter pyramidal stimulation response. This allowed for dense clusters of excitatory activity in pyramidal cells following stimulation.

In the second column to the right of the electrode array (Fig. 5*a*, column 9), we see a dense cluster of highly synchronized pyramidal layer II/III activity that was slightly delayed from the activity in the column to its left. Although pyramidal cells were no longer directly stimulated in this cortical column, this activity resulted from the rightward cross-columnar propagation of excitatory signaling. Remarkably, this substantial, synchronized pyramidal activity grew more and more synchronous as the wave propagated rightward across cortical columns. This unidirectional propagation of excitatory signaling is an exceptional product of asymmetrical stimulation (Fig. 5*a*, columns 9-11).

Following the stimulation period and initial clusters of activity that die down at ~10 ms after stimulation, there were a handful of waves of activity that ping-ponged between excitatory and inhibitory cells in columns with pyramidal excitation (Fig. 5*a*, columns 6-11). In these columns, pyramidal activity activated both Martinotti and basket cells, which in turn inhibited pyramidal activity. There were a few iterations of this negative feedback loop over the course of a few milliseconds before pyramidal spiking was halted entirely.

Analysis of synaptic currents reveals mechanism of asymmetrical spiking activity

Next, we analyzed the voltage traces of individual neurons and synaptic dynamics to explain the causes of pyramidal asymmetrical spiking activity (Fig. 6).

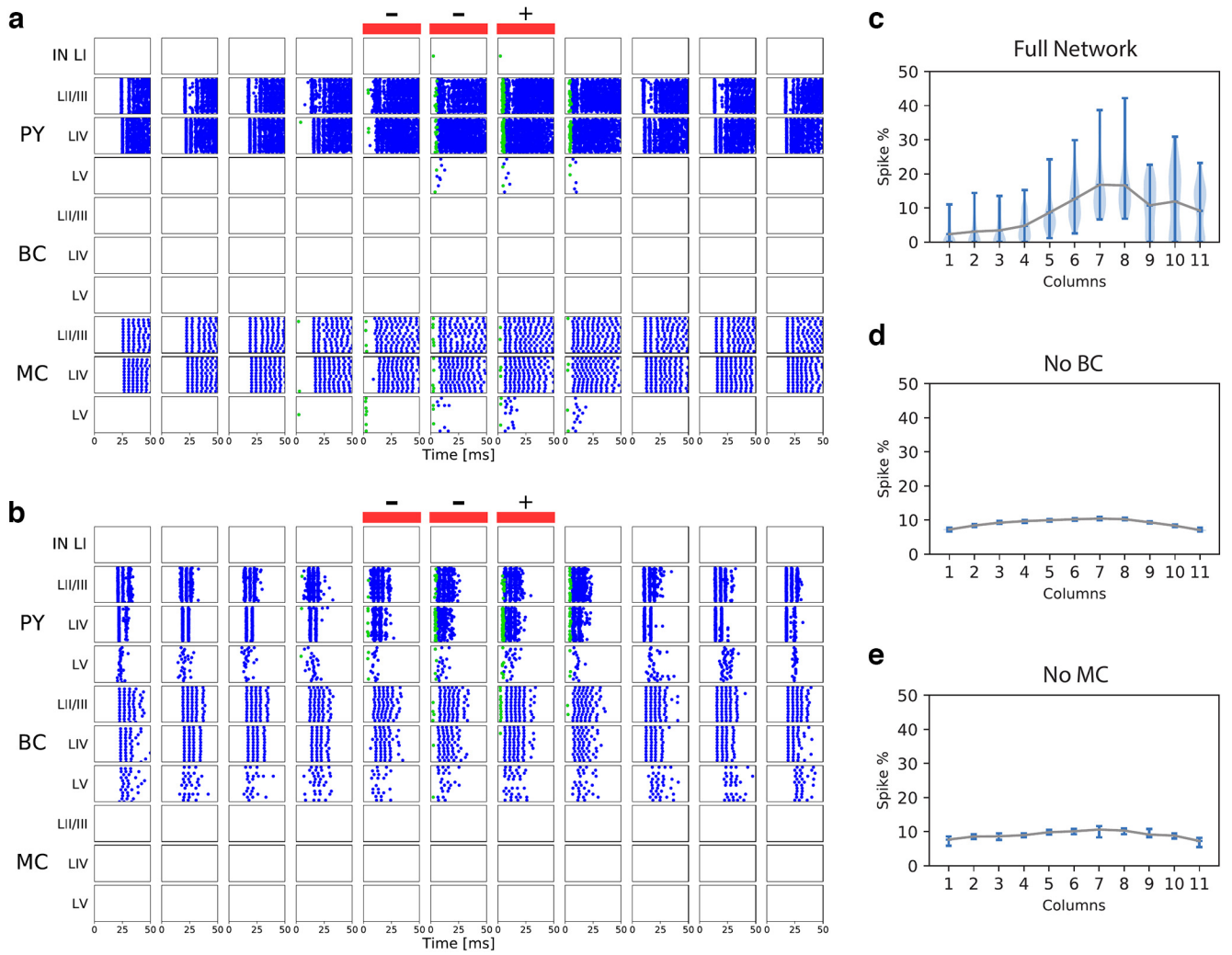

Figure 7. Cell type-specific silencing indicates distinct roles of inhibitory interneurons in temporal and spatial dynamics of the traveling wave. Raster plots displaying network activity in the same experimental setup as that shown in Figure 5*a*, except with either Basket cells (***a***) or Martinotti cells (***b***) silenced. ***c–e***, The average spike percentage per column (relative to the total number of spikes in the simulation) averaged across 20 simulations for the full network model (***c***), with silenced Basket cells (***d***), or with silenced Martinotti cells (***e***).

Voltage traces revealed that layer II/III pyramidal cells were initially depolarized underneath the anodal electrode (column 7), as they were highly activated by anodal stimulation. However, a large inhibitory conductance immediately following the stimulation period (the first g_i peak) dampened any stimulation-induced depolarization and hyperpolarized these pyramidal cells. Inhibitory conductance then fell and excitatory conductance rose as layer II/III pyramidal cells gained excitatory input from neighboring layers and columns, bringing layer II/III pyramidal cells to threshold and triggering action potentials. The second peak in inhibitory conductance midway through the pyramidal action potential was caused by pyramidal cell input into the inhibitory cells, which initiated a negative feedback loop that quickly subsided as pyramidal cells were silenced by inhibition. This effect occurred in all columns with substantial pyramidal activity.

Although there were similar inhibitory and excitatory conductance dynamics in the column underneath the central cathodal electrode (column 6), the excitatory conductance was of a smaller magnitude overall, and there were fewer action potentials because pyramidal cells were less excited by cathodal stimulation. Underneath the leftmost electrode (column 5), moderate inhibitory conductance outweighed negligible excitatory conductance, leading to minimal pyramidal activity. There was little excitation in column 4 or any of the other leftward columns (not shown). On the other side of the electrode array, in column 8, high initial excitatory conductance and minimal inhibitory conductance resulted in strong initial pyramidal spiking. Pyramidal action potentials became more and more synchronous as they traveled rightward, as evidenced by increasingly overlapped voltage traces. Together, these observations reveal the mechanisms of activity propagation to the right but not to the left in these stimulation settings.

Cell type-specific silencing reveals distinct roles of inhibitory interneurons in shaping and sustaining traveling waves

To better understand the role of basket and Martinotti cells in shaping and sustaining traveling waves, we performed cell type-specific silencing experiments using the previously described network model paradigm in Figure 5. Silencing basket cells resulted in persistent activity rapidly spreading bidirectionally from the central column similar to what may be observed during a seizure-like event (Fig. 7*a*). Compared with the control network in Figure 5*a*, without basket cells, the pyramidal cell activity within a given column never halts once initiated and appears more akin to a standing wave which spreads bidirectionally throughout the network rather than propagates. Alternatively, silencing Martinotti

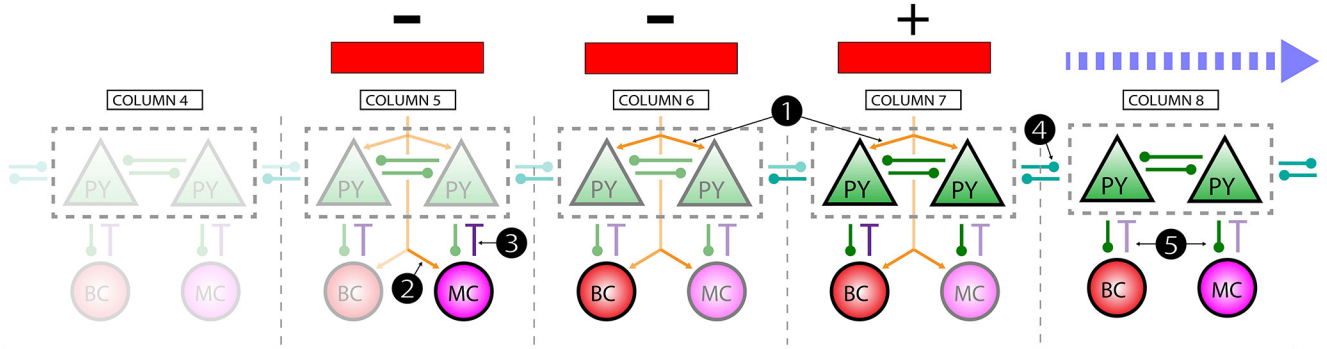

PY	No direct activation + no excitatory input + small inhibitory input = little spiking	Low direct activation + low excitatory input + moderate inhibition = low spiking	Direct activation + very little inhibition = strong spiking	Direct activation + excitatory input outweighs inhibition = strong spiking	Direct activation + high excitatory input + very low inhibition = strong spiking
BC	No direct activation + no excitatory input = little spiking	Low direct activation + low excitatory input = low spiking	Direct activation + moderate excitatory input = strong spiking	Direct activation + excitatory input = strong spiking	Strong excitatory input = strong spiking in response to PYs
MC	Small activation + no excitatory input = little spiking	High direct activation = strong initial spiking	Direct activation + moderate excitatory input = moderate spiking	Direct activation + excitatory input = moderate spiking	Excitatory input = strong spiking in response to PYs

Figure 8. Summary of interactions resulting in unidirectional propagation. Key interactions are depicted graphically above and summarized in text in the table below. Columns 4-8 of the total 11 are included, indicated by labels at top. Cell and synaptic labels are as in Figure 4. Orange arrows coming from the electrodes and pointing toward cells represent direct electrical stimulation, as opposed to synaptic inputs, indicated by the green, purple, and teal lines. The opacity of the cell labels approximately depicts the degree of spiking activity, with more transparent cells showing little or no spiking activity, and more opaque ones corresponding to more actively spiking cells. The opacity of lines indicates the strength of the input to cells, either synaptic or from the stimulating electrodes. For example, more opaque orange arrows indicate that the cell being pointed to was strongly stimulated directly. The light blue dashed arrow at the top right indicates the initiation of synchronous, unidirectional propagation of activity to the direct right of the electrodes. Key events in initiation of this unidirectional propagation are indicated by the white numbers in black circles: ① Direct activation under (+) [column 7] and central (–) [column 6] induces strong spiking in PYs, BCs, and MCs. ② Under left (–) [column 5] direct activation induces strong spiking in MCs, but little in PYs and BCs. ③ PYs in column 5 further inhibited by MCs leads to little activity to left of electrode. ④ Strong PY activity in columns 6 and 7 propagates rightward via cross-column PY-PY synapses, overcoming moderate inhibition. ⑤ PY activity causes spiking in MCs and BCs as it propagates rightward; feedback between PYs and inhibitory cells causes increasingly synchronous spiking. Layer I interneurons have been omitted, as they did not contribute significantly to the propagation described here.

cells preserved the propagating nature of the wave across columns (i.e., activity in each column self-terminated after 20-25 ms). However, this propagation was still bidirectional (Fig. 7*b*). Thus, these experiments demonstrate that both types of inhibitory cells may be necessary for the spatial asymmetry of the wave, while suggesting that basket cells may be more important for wave propagation by more effectively halting excitatory activity once initiated.

Discussion

In this work, we predict that an asymmetrical cortical stimulation protocol using a combination of anodal and cathodal electrodes may trigger propagating excitatory activity that shows strong directional preference. Our model had two steps: we first constructed a biophysical model to predict activation probabilities across cell types in response to an asymmetrically-applied electric field potential, and then incorporated these probabilities into a cortical microcircuit to model the network effects of stimulation. We found that pyramidal cells and basket cells are highly activated by the anodal electrode and minimally activated by the cathodal electrodes because of their myelination and horizontal axonal arbors, while layer I interneurons are only moderately activated by the anodal electrode despite their horizontal axonal arbors due to lack of myelination. Martinotti cells also exhibit moderate activation due to lack on myelination, but show a slight preference for cathodal stimulation due to their predominately vertically-oriented axonal arbors. Network model simulations revealed that this asymmetrical activation results in a traveling wave in superficial excitatory cells that propagates away from the electrode array, past the anodal electrode, and into adjacent cortical columns, but does not propagate in the opposite direction past the leftmost cathodal electrodes (Fig. 8).

We found that distinct classes of inhibitory cells are the cause of separable components of the unidirectional propagation. Basket cells were necessary for the wave to propagate (as opposed to spread as a standing wave), but both basket and Martinotti cells were needed for asymmetrical spatial propagation. While activity directly under the central column is defined by the stimulation protocol, as the activity propagates laterally through horizontal excitatory connections, the increasing synchrony of cell firing is likely mediated by a PING type mechanism (Whittington et al., 2000) (Martinotti cells were not necessary for this aspect of the activity, as shown in Figure 7*b*).

Importantly, only the spatial component of the traveling wave is dependent on the particular electrode design of the stimulation paradigm; the temporal component is a manifestation of endogenous cortical columnar circuitry. This allows for endogenous oscillatory activity to be spatially guided through the network, without inducing artificial frequencies as a result of stimulation. These two classes of inhibitory cells could be deactivated optogenetically in rodents during stimulation to test the predictions of the model. Electrical stimulation paradigms that rely on current steering to guide activity along particular trajectories are widely used both experimentally and clinically and have demonstrated robust efficacy at the macroscopic network level, but are still poorly understood at the mesoscopic circuit level. Ultimately, we believe that this model is a first step toward understanding the circuit mechanisms which are engaged during these stimulation practices.

Traveling waves in the brain

Multielectrode recordings in human and animal subjects have demonstrated the ubiquity of traveling waves in cognitive

function (Muller et al., 2018). They relay information across a range of distances and thereby coordinate fundamental processes such as memory, perception, language, orientation, executive functions, and more across distant brain regions (Rubino et al., 2006; Wu et al., 2008; Muller et al., 2018; Salimpour and Anderson, 2019). Recordings have also shown that propagating activity present in the human cortex is often directional, traveling from one point to another. The ability to generate directional propagation via stimulation would allow for unique precision in and control over induced activity. This has widespread implications for the restoration or enhancement of high-level brain function, particularly because many neuropsychiatric disorders are marked by abnormal or absent propagating activity.

In the model, propagating activity was confined to supragranular cortical layers. This may not be a limitation if the goal is to reproduce natural waves, because spontaneous traveling waves in the human cortex have also been found to be largely confined to upper layers, including the alpha rhythm during waking (M. Halgren et al., 2019), and spindles and slow oscillation during sleep (Cash et al., 2009; M. Halgren et al., 2018).

Traveling waves have long been studied with a variety of computational models, and numerous mechanisms have been proposed to explain how activity propagates across neuronal networks (Ermentrout and Kleinfeld, 2001; Breakspear, 2017). Cortical propagating waves that are triggered specifically by electrical stimulation have been recorded in mammalian cortical slices (Kim et al., 1995; Wu et al., 2001; Wester and Contreras, 2012), as well as in non-human mammals (Contreras et al., 1997; Xu et al., 2007; Stieger et al., 2020) and simulated in non-mammalian computational models (Chen et al., 2008), but remain understudied in human subjects. This previous experimental work, both *in vivo* and *in silico*, has yielded scarce evidence of asymmetrical traveling wave propagation or reliable wave generation analogous to that reported here. To the extent that previous work has focused on traveling wave propagation initiated by stimulation (Alekseichuk et al., 2019), these studies examined stimulation through the skull and meninges, and are thus not directly comparable to this model of intracranial stimulation of the cortical surface. Many computational models exist that model the effects of stimulation on the brain, including some that have constructed Hodgkin–Huxley microcircuits (Douglas et al., 1995; Haeusler and Maass, 2007) and modeled cortical surface stimulation (Anderson et al., 2009). However, few have modeled multielectrode or asymmetrical stimulation or reproduced traveling waves using surface electrodes. Many existing stimulation models have focused on stimulation of a particular nerve (Raspopovic et al., 2011; Helmers et al., 2012) or an isolated cell type (Traub et al., 1994; R. J. Greenberg et al., 1999), as opposed to the functioning cortical microcircuit presented here, which can be more readily adapted to other cortical regions by adjusting the parameters and neuronal reconstructions used. In addition, stimulation has more often been simulated in these models by a simple application of suprathreshold current or a uniform electric field (Radman et al., 2007, 2009). Thus, by combining the two-phase biophysical model with asymmetrical, multipolar surface stimulation, our approach synthesizes existing achievements into a single coherent, clinically-adaptable model that uniquely sheds light on the generation of propagating wave activity.

Clinical relevance of our findings

Brain stimulation is becoming increasingly common in clinical and experimental settings, especially using multielectrode arrays (Lewis et al., 2015). As such, it is pressing that we develop accurate models of the effects that multielectrode stimulation has on neural activity. While sometimes the explicit goal of stimulation may be to disrupt aberrant activity to restore normal functioning, increasingly the goal is to induce the desired brain activity directly via stimulation, as our work demonstrates.

Changes in neural plasticity result from patterned activity, with the particular changes in connectivity contingent on the specific timing and order of activity (Bennett and Bair, 2015). Stimulation protocols that induce neural activity which continues past the stimulus duration are more likely to alter cellular and synaptic properties in favor of the induced activity, in contrast to stimulation protocols that briefly activate broad swaths of cells without triggering existing activity patterns. Thus, initiating propagating waves within tailored spatiotemporal constraints is a promising way to retrain neural networks and enhance or silence brain functions in a targeted way.

The generation of traveling waves may serve as a promising therapy for a variety of neurological disorders. For example, it has been previously suggested that triggering propagating activity in perilesional areas where waves are otherwise aberrant or absent may be an effective therapy for post-stroke aphasia (Beuter et al., 2020). While the ultimate clinical applications of this technique are uncertain, stimulation-induced traveling waves may have the potential to offset inhibition in cortical spreading depression (Liebetanz et al., 2006; Santos et al., 2012), reduce the risk of seizure while determining which brain tissue to remove from epilepsy patients (Nagaraj et al., 2015), and enhance memory formation when applied during learning or recall periods (Suthana et al., 2012; Batterink et al., 2016; Ezzyat et al., 2018; Kucewicz et al., 2018a,b), as consistency in traveling wave direction is positively correlated with working memory efficiency (Zhang et al., 2018).

Limitations

In this work, we modeled a single, short stimulating pulse. However, clinical stimulation is most often composed of longer pulses or pulse trains and is usually performed with bipolar electrodes delivering biphasic pulses to prevent damaging Faradic currents (Merrill et al., 2005; Cogan et al., 2016). These stimulation paradigms modulate properties over time that are not accounted for in the current model, such as underlying dendritic and axonal dynamics as well as synaptic interactions. Thus, our biophysical approach may be expanded in future studies to incorporate these steady-state properties through alternative modeling approaches, such as the cylinder model (Rall, 1962; Tranchina and Nicholson, 1986) or the multicompartmental model (Berzhanskaya et al., 2013). However, we chose to model the activation probability of the axonal instead of the dendritic arbor in this work because experimental evidence shows that the nodes of Ranvier, followed by the axon hillock, are the most excitable neuronal elements by far via direct stimulation (Gustafsson and Jankowska, 1976; Swadlow, 1992; Rattay, 1999; Tehovnik et al., 2006) as they both have a high concentration of sodium channels (Catterall, 1981). In contrast, direct stimulation of the dendritic arbor generates transmembrane currents that propagate to the axon hillock, but these effects are strongly attenuated and delayed, and are negligible compared with direct stimulation of the nodes of Ranvier and axon hillock.

Consistent with the findings that the axon is the most likely site of action potential initiation under electrical stimulation, our approach has focused specifically on estimating this probability while neglecting other aspects of stimulation which may alter

subsequent network activity. In particular, effects of stimulation on nonlinear, often calcium-mediated, properties of the dendrites and axon terminals would be expected to significantly outlast the duration of stimulation. Both of these locations can directly influence synaptic efficacy, or even decorrelate synaptic release from action potential initiation (Katz and Miledi, 1967), and therefore could substantially alter subsequent network dynamics in neural tissue.

Moreover, previous modeling studies have indicated that the most depolarized neural element is not always the site of action potential initiation (McIntyre and Grill, 1999). This was particularly found to be the case when the electrode was positioned near the cell body, which resulted in maximal depolarization in the dendrites or soma, but with action potential initiation taking place in the axon or at the initial segment. For the present study, this breakdown in the assumptions of the activating function approach is mitigated by the more proximal relationship of the axons than the soma to the electrode and the short pulse duration, as such conditions have been found to show greater correspondence between the site of maximal depolarization and action potential initiation, both of which typically occurred in axonal segments (Rattay and Aberham, 1993; McIntyre and Grill, 1999). In future studies which consider longer stimulus durations or DBS paradigms where the electrode may be more proximal to the soma than axonal – conditions that are particularly pertinent to clinical applications – an active cable theory model would need to be used to properly account for action potential initiation.

In the microcircuit phase of the model, the connectivity between different cell types follows a canonical microcircuit model. While this approach characterizes the main signal pathways and feedback loops present within cortical columns (Douglas et al., 1989; da Costa and Martin, 2010; Defelipe et al., 2012), finer details are not modeled, such as descending projections to inhibitory cells from excitatory cells (Thomson et al., 2002) or the contribution of less common interneuron cell types. The cells within the cortical microcircuit model could be extended from single-compartment to multicompartment neurons (Bonjean et al., 2012) to distinguish tuft versus soma-targeting interneurons, which may further differentiate the inhibitory power of interneuron cell types (Markram et al., 2004). This phase of the model may be further expanded from a 2D plane to a 3D circuit in the volume of cortex underneath the electrodes to understand how activity spreads across space.

While moving to multicompartment neurons with active properties would alleviate many of the limitations of our approach discussed above, it also presents unique difficulties. Such models are vastly higher-dimensional than the passive cable and point-neuron models considered here and are difficult to properly constrain because of the lack of experimental data on the distribution of passive and active ion channels within different cell types necessary for data-driven parameterization. Without such constraints, these high-dimensional models are liable to be finely tuned within their vast parameter space to be able to exhibit nearly any desired activity and run the risk of diverging from biologically realistic parameter regimens and decoupling the modeled activity from plausible cellular mechanisms. Given that our goal in this study was to shed light on the cellular and circuit mechanisms underlying electrical stimulation and current steering rather than provide robust statistical predictions of the results of this particular electrical stimulation design, we opted to use models which, although known to be incomplete, are capable of more robustly constrained parameterization.

Alternative modeling approaches

In this modeling work, we have focused on estimating transient, cell type-specific responses to electrical stimulation, and subsequently incorporated these estimates into a biophysical network model of the canonical cortical column. In this sense, we directly model certain effects of electrical stimulation at the microscopic, cellular level, and then import these findings into a mesoscopic, cortical circuit model. Previous work has approached the problem of modeling the effects of electrical stimulation in diverse ways at multiple scales. At the microscopic level, McIntyre et al. (2004a) used a multicompartmental cable theory model with active properties to study the effect of DBS on the cellular properties of single thalamocortical relay neurons (McIntyre et al., 2004a). More recently, such an approach was used to study single-cell responses to intracortical and uniform electric field stimulation for a variety of cell types obtained from human and rat cortical neuron reconstructions (Aberra et al., 2018). At more macroscopic levels, researchers have used finite-element methods to model epidural electrical stimulation of the motor cortex which can account for cortical folding (Wongsarnpigoon and Grill, 2008, 2012; Aberra et al., 2018), and have incorporated data from human diffusion tensor MRI to estimate the volume of tissue activated by DBS in the subthalamic nucleus (McIntyre et al., 2004b).

Generalization of this approach

While this work modeled a specific stimulation protocol for a particular and still simplified cortical network architecture, the approach is generalizable to a variety of basic science and clinical applications. This versatility comes from the modular structure of the model, which completely decouples the biophysical-anatomical model from the dynamic-neuronal network model. This makes it possible to use the same activation probabilities for a variety of network models so long as they contain analogs of the initial cell types. Additionally, circumventing the computational complexity of simulating high-dimensional compartmental models facilitates the widespread investigation of much larger networks than studied in this paper. Indeed, recent empirical studies have collected an enormous amount of new data regarding cell properties and local- and long-range connectivity, but current modeling efforts have yet to take advantage of these data. It is still not feasible to simulate large-scale network models, including different brain structures (Sanda et al., 2021) and/or multiple cortical regions and long-range connectivity (Rosen et al., 2019), which would be built on anatomically realistic cell reconstructions and include multiple layers and different cell types. This severely limits how new anatomical and functional data are used in the model design, and we suggest that the hybrid approach we present here may help to partially overcome these limitations.

In conclusion, this work models an asymmetrical stimulation paradigm that could be implemented to initiate unidirectional traveling waves in the cortex. A biophysical model is integrated with a computational network model to predict the behavior of single neurons as well as the cortical network dynamics resulting from multielectrode stimulation. This model provides hypotheses and stimulation paradigms which can be verified experimentally. It expands on the capabilities of our hybrid modeling approach to show how it can be deployed to probe the relationship between the microscale effects of electrical stimulation and the mesoscale consequences at the level of circuit dynamics. These results demonstrate how complex stimulation protocols

could be harnessed to generate persistent changes in activity with the potential to restore normal brain function in neurological and psychiatric conditions.

References

Abelson JL, Curtis GC, Sagher O, Albucher RC, Harrigan M, Taylor SF, Martis B, Giordani B (2005) Deep brain stimulation for refractory obsessive-compulsive disorder. Biol Psychiatry 57:510–516.

Aberra AS, Peterchev AV, Grill WM (2018) Biophysically realistic neuron models for simulation of cortical stimulation. J Neural Eng 15:066023.

Alekseichuk I, Falchier AY, Linn G, Xu T, Milham MP, Schroeder CE, Opitz A (2019) Electric field dynamics in the brain during multi-electrode transcranial electric stimulation. Nat Commun 10:2573.

Anderson WS, Kudela P, Weinberg S, Bergey GK, Franaszczuk PJ (2009) Phase-dependent stimulation effects on bursting activity in a neural network cortical simulation. Epilepsy Res 84:42–55.

Ascoli GA, Donohue DE, Halavi M (2007) NeuroMorpho.Org: a central resource for neuronal morphologies. J Neurosci 27:9247–9251.

Baizabal-Carvallo JF, Alonso-Juarez M (2016) Low-frequency deep brain stimulation for movement disorders. Parkinsonism Relat Disord 31:14–22.

Batterink LJ, Creery JD, Paller KA (2016) Phase of spontaneous slow oscillations during sleep influences memory-related processing of auditory cues. J Neurosci 36:1401–1409.

Bennett JE, Bair W (2015) Refinement and pattern formation in neural circuits by the interaction of traveling waves with spike timing-dependent plasticity. PLoS Comput Biol 11:e1004422.

Berzhanskaya J, Chernyy N, Gluckman BJ, Schiff SJ, Ascoli GA (2013) Modulation of hippocampal rhythms by subthreshold electric fields and network topology. J Comput Neurosci 34:369–389.

Beuter A, Balossier A, Vassal F, Hemm S, Volpert V (2020) Cortical stimulation in aphasia following ischemic stroke: toward model-guided electrical neuromodulation. Biol Cybern 114:5–21.

Blumenfeld Z, Bronte-Stewart H (2015) High frequency deep brain stimulation and neural rhythms in Parkinson's disease. Neuropsychol Rev 25:384–397.

Bonjean M, Baker T, Bazhenov M, Cash S, Halgren E, Sejnowski T (2012) Interactions between core and matrix thalamocortical projections in human sleep spindle synchronization. J Neurosci 32:5250–5263.

Breakspear M (2017) Dynamic models of large-scale brain activity. Nat Neurosci 20:340–352.

Cash SS, Halgren E, Dehghani N, Rossetti AO, Thesen T, Wang C, Devinsky O, Kuzniecky R, Doyle W, Madsen JR, Bromfield E, Eross L, Halasz P, Karmos G, Csercsa R, Wittner L, Ulbert I (2009) The human K-complex represents an isolated cortical down-state. Science 324:1084–1087.

Catterall WA (1981) Localization of sodium channels in cultured neural cells. J Neurosci 1:777–783.

Chen E, Stiefel KM, Sejnowski TJ, Bullock TH (2008) Model of traveling waves in a coral nerve network. J Comp Physiol A Neuroethol Sens Neural Behav Physiol 194:195–200.

Cogan SF, Ludwig KA, Welle CG, Takmakov P (2016) Tissue damage thresholds during therapeutic electrical stimulation. J Neural Eng 13:021001.

Contreras D, Destexhe A, Sejnowski TJ, Steriade M (1997) Spatiotemporal patterns of spindle oscillations in cortex and thalamus. J Neurosci 17:1179–1196.

da Costa NM, Martin KAC (2010) Whose cortical column would that be? Front Neuroanat 4:16.

Defelipe J, Markram H, Rockland KS (2012) The neocortical column. Front Neuroanat 6:22.

Dickey CW, Sargsyan A, Madsen JR, Eskandar EN, Cash SS, Halgren E (2021) Travelling spindles create necessary conditions for spike-timing-dependent plasticity in humans. Nat Commun 12:1027.

Douglas RJ, Martin KAC (1991) A functional microcircuit for cat visual cortex. J Physiol 440:735–769.

Douglas RJ, Martin KAC, Whitteridge D (1989) A canonical microcircuit for neocortex. Neural Comput 1:480–488.

Douglas RJ, Koch C, Mahowald M, Martin KAC, Suarez HH (1995) Recurrent excitation in neocortical circuits. Science 269:981–985.

Ermentrout GB, Kleinfeld D (2001) Traveling electrical waves in cortex: insights from phase dynamics and speculation on a computational role. Neuron 29:33–44.

Ezzyat Y, et al. (2018) Closed-loop stimulation of temporal cortex rescues functional networks and improves memory. Nat Commun 9:365.

Greenberg BD, Malone DA, Friehs GM, Rezai AR, Kubu CS, Malloy PF, Salloway SP, Okun MS, Goodman WK, Rasmussen SA (2006) Three-year outcomes in deep brain stimulation for highly resistant obsessive-compulsive disorder. Neuropsychopharmacology 31:2384–2393.

Greenberg RJ, Velte TJ, Humayun MS, Scarlatis GN, de Juan E Jr (1999) A computational model of electrical stimulation of the retinal ganglion cell. IEEE Trans Biomed Eng 46:505–514.

Gustafsson B, Jankowska E (1976) Direct and indirect activation of nerve cells by electrical pulses applied extracellularly. J Physiol 258:33–61.

Ha S, Akinin A, Park AJ, Kim C, Wang H, Maier C, Mercier P, Cauwenberghs G (2017) Silicon-integrated high-density electrocortical interfaces. Proc IEEE 105:11–33.

Haeusler S, Maass W (2007) A statistical analysis of information-processing properties of lamina-specific cortical microcircuit models. Cereb Cortex 17:149–162.

Halgren E, Walter RD, Cherlow DG, Crandall PH (1978) Mental phenomena evoked by electrical stimulation of the human hippocampal formation and amygdala. Brain 101:83–115.

Halgren M, Fabo D, Ulbert I, Madsen JR, Eross L, Doyle WK, Devinsky O, Schomer D, Cash SS, Halgren E (2018) Superficial slow rhythms integrate cortical processing in humans. Sci Rep 8:2055.

Halgren M, Ulbert I, Bastuji H, Fabo D, Eross L, Rey M, Devinsky O, Doyle WK, Mak-McCully R, Halgren E, Wittner L, Chauvel P, Heit G, Eskandar E, Mandell A, Cash SS (2019) The generation and propagation of the human alpha rhythm. Proc Natl Acad Sci USA 116:23772–23782.

Helmers SL, Begnaud J, Cowley A, Corwin HM, Edwards JC, Holder DL, Kostov H, Larsson PG, Levisohn PM, De Menezes MS, Stefan H, Labiner DM (2012) Application of a computational model of vagus nerve stimulation. Acta Neurol Scand 126:336–343.

Hummel FC, Cohen LG (2006) Non-invasive brain stimulation: a new strategy to improve neurorehabilitation after stroke? Lancet Neurol 5:708–712.

Kahana MJ, Aggarwal EV, Phan TD (2018) The variability puzzle in human memory. J Exp Psychol Learn Mem Cogn 44:1857–1863.

Katz B, Miledi R (1967) A study of synaptic transmission in the absence of nerve impulses. J Physiol 192:407–436.

Kim U, Bal T, McCormick DA (1995) Spindle waves are propagating synchronized oscillations in the ferret LGNd in vitro. J Neurophysiol 74:1301–1323.

Komarov M, Malerba P, Golden R, Nunez P, Halgren E, Bazhenov M (2019) Selective recruitment of cortical neurons by electrical stimulation. PLoS Comput Biol 15:e1007277.

Kucewicz MT, Berry BM, Kremen V, Miller LR, Khadjevand F, Ezzyat Y, Stein JM, Wanda P, Sperling MR, Gorniak R, Davis KA, Jobst BC, Gross RE, Lega B, Stead SM, Rizzuto DS, Kahana MJ, Worrell GA (2018a) Electrical stimulation modulates high gamma activity and human memory performance. eNeuro 5:ENEURO.0369-17.2018.

Kucewicz MT, Berry BM, Miller LR, Khadjevand F, Ezzyat Y, Stein JM, Kremen V, Brinkmann BH, Wanda P, Sperling MR, Gorniak R, Davis KA, Jobst BC, Gross RE, Lega B, Van Gompel J, Stead SM, Rizzuto DS, Kahana MJ, Worrell GA (2018b) Evidence for verbal memory enhancement with electrical brain stimulation in the lateral temporal cortex. Brain 141:971–978.

Lewis PM, Ackland HM, Lowery AJ, Rosenfeld JV (2015) Restoration of vision in blind individuals using bionic devices: a review with a focus on cortical visual prostheses. Brain Res 1595:51–73.

Liebetanz D, Fregni F, Monte-Silva KK, Oliveira MB, Amancio-dos-Santos A, Nitsche MA, Guedes RC (2006) After-effects of transcranial direct current stimulation (tDCS) on cortical spreading depression. Neurosci Lett 398:85–90.

Markram H, Toledo-Rodriguez M, Wang Y, Gupta A, Silberberg G, Wu C (2004) Interneurons of the neocortical inhibitory system. Nat Rev Neurosci 5:793–807.

Mayberg HS, Lozano AM, Voon V, McNeely HE, Seminowicz D, Hamani C, Schwalb JM, Kennedy SH (2005) Deep brain stimulation for treatment-resistant depression. Neuron 45:651–660.

McIntyre CC, Grill WM (1999) Excitation of central nervous system neurons by nonuniform electric fields. Biophys J 76:878–888.

McIntyre CC, Grill WM, Sherman DL, Thakor NV (2004a) Cellular effects of deep brain stimulation: model-based analysis of activation and inhibition. J Neurophysiol 91:1457–1469.

McIntyre CC, Mori S, Sherman DL, Thakor NV, Vitek JL (2004b) Electric field and stimulating influence generated by deep brain stimulation of the subthalamic nucleus. Clin Neurophysiol 115:589–595.

Merrill DR, Bikson M, Jefferys JG (2005) Electrical stimulation of excitable tissue: design of efficacious and safe protocols. J Neurosci Methods 141:171–198.

Muller L, Chavane F, Reynolds J, Sejnowski TJ (2018) Cortical travelling waves: mechanisms and computational principles. Nat Rev Neurosci 19:255–268.

Muralidhar S, Wang Y, Markram H (2013) Synaptic and cellular organization of layer 1 of the developing rat somatosensory cortex. Front Neuroanat 7:52.

Nagaraj V, Lee ST, Krook-Magnuson E, Soltesz I, Benquet P, Irazoqui PP, Netoff TI (2015) Future of seizure prediction and intervention: closing the loop. J Clin Neurophysiol 32:194–206.

Papageorgiou PN, Deschner J, Papageorgiou SN (2017) Effectiveness and adverse effects of deep brain stimulation: umbrella review of meta-analyses. J Neurol Surg A Cent Eur Neurosurg 78:180–190.

Radman T, Su Y, An JH, Parra LC, Bikson M (2007) Spike timing amplifies the effect of electric fields on neurons: implications for endogenous field effects. J Neurosci 27:3030–3036.

Radman T, Ramos RL, Brumberg JC, Bikson M (2009) Role of cortical cell type and morphology in subthreshold and suprathreshold uniform electric field stimulation in vitro. Brain Stimul 2:215–228.e3.

Rall W (1962) Electrophysiology of a dendritic neuron model. Biophys J 2:145–167.

Raspopovic S, Capogrosso M, Micera S (2011) A computational model for the stimulation of rat sciatic nerve using a transverse intrafascicular multichannel electrode. IEEE Trans Neural Syst Rehabil Eng 19:333–344.

Rattay F (1999) The basic mechanism for the electrical stimulation of the nervous system. Neuroscience 89:335–346.

Rattay F, Aberham M (1993) Modeling axon membranes for functional electrical stimulation. IEEE Trans Biomed Eng 40:1201–1209.

Rosen BQ, Krishnan GP, Sanda P, Komarov M, Sejnowski T, Rulkov N, Ulbert I, Eross L, Madsen J, Devinsky O, Doyle W, Fabo D, Cash S, Bazhenov M, Halgren E (2019) Simulating human sleep spindle MEG and EEG from ion channel and circuit level dynamics. J Neurosci Methods 316:46–57.

Rubino D, Robbins KA, Hatsopoulos NG (2006) Propagating waves mediate information transfer in the motor cortex. Nat Neurosci 9:1549–1557.

Salimpour Y, Anderson WS (2019) Cross-frequency coupling based neuromodulation for treating neurological disorders. Front Neurosci 13:125.

Salzman CD, Britten KH, Newsome WT (1990) Cortical microstimulation influences perceptual judgements of motion direction. Nature 346:174–177.

Sanda P, Malerba P, Jiang X, Krishnan GP, Gonzalez-Martinez J, Halgren E, Bazhenov M (2021) Bidirectional interaction of hippocampal ripples and cortical slow waves leads to coordinated spiking activity during NREM sleep. Cereb Cortex 31:324–340.

Santos E, Sanchez-Porras R, Dohmen C, Hertle D, Unterberg AW, Sakowitz OW (2012) Spreading depolarizations in a case of migraine-related stroke. Cephalalgia 32:433–436.

Schlaepfer TE, Cohen MX, Frick C, Kosel M, Brodesser D, Axmacher N, Joe AY, Kreft M, Lenartz D, Sturm V (2008) Deep brain stimulation to reward circuitry alleviates anhedonia in refractory major depression. Neuropsychopharmacology 33:368–377.

Schubert D, Kotter R, Luhmann HJ, Staiger JF (2006) Morphology, electrophysiology and functional input connectivity of pyramidal neurons characterizes a genuine layer Va in the primary somatosensory cortex. Cereb Cortex 16:223–236.

Staiger JF, Flagmeyer I, Schubert D, Zilles K, Kotter R, Luhmann HJ (2004) Functional diversity of layer IV spiny neurons in rat somatosensory cortex: quantitative morphology of electrophysiologically characterized and biocytin labeled cells. Cereb Cortex 14:690–701.

Stieger KC, Eles JR, Ludwig KA, Kozai TD (2020) In vivo microstimulation with cathodic and anodic asymmetric waveforms modulates spatiotemporal calcium dynamics in cortical neuropil and pyramidal neurons of male mice. J Neurosci Res 98:2072–2095.

Suthana N, Haneef Z, Stern J, Mukamel R, Behnke E, Knowlton B, Fried I (2012) Memory enhancement and deep-brain stimulation of the entorhinal area. N Engl J Med 366:502–510.

Swadlow HA (1992) Monitoring the excitability of neocortical efferent neurons to direct activation by extracellular current pulses. J Neurophysiol 68:605–619.

Tehovnik EJ, Slocum WM, Schiller PH (2002) Differential effects of laminar stimulation of V1 cortex on target selection by macaque monkeys. Eur J Neurosci 16:751–760.

Tehovnik EJ, Tolias AS, Sultan F, Slocum WM, Logothetis NK (2006) Direct and indirect activation of cortical neurons by electrical microstimulation. J Neurophysiol 96:512–521.

Thomson AM, West DC, Wang Y, Bannister AP (2002) Synaptic connections and small circuits involving excitatory and inhibitory neurons in layers 2-5 of adult rat and cat neocortex: triple intracellular recordings and biocytin labelling in vitro. Cereb Cortex 12:936–953.

Tomassy GS, Berger DR, Chen HH, Kasthuri N, Hayworth KJ, Vercelli A, Seung HS, Lichtman JW, Arlotta P (2014) Distinct profiles of myelin distribution along single axons of pyramidal neurons in the neocortex. Science 344:319–324.

Tranchina D, Nicholson C (1986) A model for the polarization of neurons by extrinsically applied electric fields. Biophys J 50:1139–1156.

Traub RD, Jefferys JG, Miles R, Whittington MA, Toth K (1994) A branching dendritic model of a rodent CA3 pyramidal neurone. J Physiol 481:79–95.

Wang Y, Gupta A, Toledo-Rodriguez M, Wu CZ, Markram H (2002) Anatomical, physiological, molecular and circuit properties of nest basket cells in the developing somatosensory cortex. Cereb Cortex 12:395–410.

Wang Y, Toledo-Rodriguez M, Gupta A, Wu C, Silberberg G, Luo J, Markram H (2004) Anatomical, physiological and molecular properties of Martinotti cells in the somatosensory cortex of the juvenile rat. J Physiol 561:65–90.

Wester JC, Contreras D (2012) Columnar interactions determine horizontal propagation of recurrent network activity in neocortex. J Neurosci 32:5454–5471.

Whittington MA, Traub RD, Kopell N, Ermentrout B, Buhl EH (2000) Inhibition-based rhythms: experimental and mathematical observations on network dynamics. Int J Psychophysiol 38:315–336.

Wongsarnpigoon A, Grill WM (2008) Computational modeling of epidural cortical stimulation. J Neural Eng 5:443–454.

Wongsarnpigoon A, Grill WM (2012) Computer-based model of epidural motor cortex stimulation: effects of electrode position and geometry on activation of cortical neurons. Clin Neurophysiol 123:160–172.

Wu JY, Guan L, Bai L, Yang Q (2001) Spatiotemporal properties of an evoked population activity in rat sensory cortical slices. J Neurophysiol 86:2461–2474.

Wu JY, Xiaoying H, Chuan Z (2008) Propagating waves of activity in the neocortex: what they are, what they do. Neuroscientist 14:487–502.

Xu W, Huang X, Takagaki K, Wu JY (2007) Compression and reflection of visually evoked cortical waves. Neuron 55:119–129.

Zhang H, Watrous AJ, Patel A, Jacobs J (2018) Theta and alpha oscillations are traveling waves in the human neocortex. Neuron 98:1269–1281.e4.